Int. J. Electrochem. Sci., 12 **(2017)** 4915 – 4927, doi: 10.20964/2017.06.76

International Journal of ELECTROCHEMICAL SCIENCE
www.electrochemsci.org

Mini Review

Recent Research Progress on Lead-free or Less-lead Perovskite Solar Cells

Qihua Li, Peixin Zhang, Lei Yao, Libo Deng[*]*, Xiangzhong Ren and Yongliang Li*

College of Chemistry and Environmental Engineering, Shenzhen University, Shenzhen 518060, China
[*]E-mail: Denglb@szu.edu.cn

Received: 2 September 2016 / *Accepted:* 13 April 2017 / *Published:* 12 May 2017

Perovskite solar cells (PSCs) have been attracting great research interests and attained remarkable progress since its debut in 2009. Remarkably, the power conversion efficiency (PCE) of PSCs has already surpassed other types of solar cells that have been researched over 20 years in the last 7 years. However, organic lead halides are extensively used as absorption materials of current PSCs, which are toxic and environment-unfriendly and hinder the practical applications of PSCs. For these reasons, research on less-lead or lead-free PSCs is of great importance. Tin is an ideal substitution to lead because it is nontoxic and the absorption spectra of some of the tin-based perovskites are broader than lead-based perovskites. However, tin-based perovskite materials are more prone to be oxidized than organic lead halide perovskite, which would result in a lower PCE and poorer stability for tin-based PSCs than those for the organic halide lead PSCs. Therefore, it is necessary to further optimize the less-lead or lead-free perovskite materials and fabricate efficient, stable and environmental friendly PSCs. Recent research progress on less-lead and lead-free PSCs is summarized in this mini review and the possible solutions to the issues regarding the photoelectric performance and stability are proposed.

Keywords: Perovskite solar cells; less-lead; lead-free; tin-based perovskite

1. INTRODUCTION

As one of the main methods to solve the energy crisis, solar cells received increasingly attention in the last decades [1-5]. Particularly, research on PSCs attained significant achievements recently [6]. In 2009, Miyasaka et al. utilized organic metal halide perovskite $CH_3NH_3PbI_3$ as sensitizer to fabricate dye-sensitized solar cells (DSSCs) that attained an efficiency of 3.8% [7], which was the first report for application of perovskite as the light-absorption materials in solar cells. However, the efficiency of the first PSCs decreases rapidly due to that perovskite is readily dissolved in the liquid electrolyte. To this end, Grätzel et al. used 2,2',7,7'-tetrakis(*N*,*N*-p-dimethoxy-

phenylamino)-9,9'-spirobifluorene (Spiro-OMeTAD) as the hole solid electrolyte to replace the liquid electrolyte. Not only did the cells achieved a PCE of 9.7% [8], but also the stability was signifcantly enhanced. Since the use of Spiro-OMeTAD as the electrolyte and also called hole transporting material (HTM), PSCs have attracted numerous attention and the PCE of PSCs attained remarkable improvements [9-21]. The development of PCE and research achievement are shown in Figure 1 [22, 23]. Recently, the highest efficiency of PSCs has reached 21.1% [24].

So far, the light-absorption material of most efficient PSCs is lead-based perovskite. Nevertheless, the toxic element lead endangers human's health and leads to environmental pollution during its fabrication and application [25]. As the optimum substitution absorption material, the band gap of the tin-based perovskite is narrower while the absorption range is wider than the lead-based perovskite. Therefore, some types of tin-based perovskites exhibit superior photoelectric performances compared to organic lead halide perovskite. However, some issues still exist in tin-based PSCs such as the high sensitivity to moisture and oxygen leading their readily oxidation at ambient condition, causing a poor stability and far lower PCEs than the organic lead halide PSCs. Although the recent progress on PSCs and its fabrication have been summarized by numerous researchers [26-36], there are no reports summarizing the progress on less-lead and lead-free PSCs so far. By reviewing the researches on the less-lead and lead-free PSCs, some issues that occurred in less-lead and lead-free PSCs and corresponding solutions are discussed.

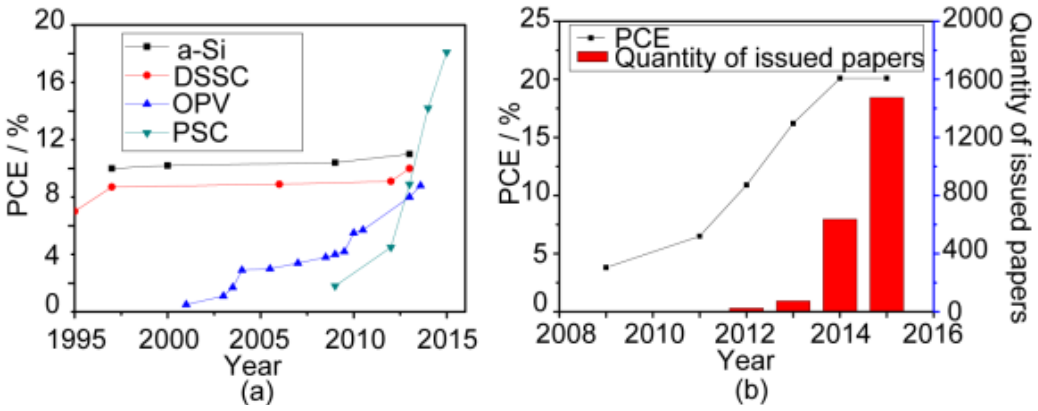

Figure 1. (a) The efficiency development of different solar cells and (b) the number of paper published on PSCs over the last seven years. (Reproduced with permission from ref. [22, 23]).

2. STRUCTURE AND WORKING PRINCIPLE OF PSCS

2.1. Structure of PSCs

The PSCs are generally classified into two types according to the structure, i.e. meso-structured PSCs and planar heterojunction PSCs, both containing a conducting substrate, an electron transporting layer (ETL), a light-absorption layer, a hole transporting layer (HTL) and a counter electrode. The schematic of the PSCs structure is shown in Figure 2 [32]. The structural diagram of meso-structured

PSCs is shown in Figure 2(a). In a typical fabrication process, a compact TiO_2 layer that not only transfers photoelectron but also hinders the recombination of photoelectron and hole is first spin-coated on the conducting substrate such as fluorine doped tin oxide (FTO). On the top of FTO/compact TiO_2 layer, a mesoporous TiO_2 layer is fabricated by the method of spin-coating or screen printing and the perovskite light-absorption material crystal grows on the scaffold of mesoporous TiO_2 [37]. The HTM is applied by spin-coating after the deposition of perovskite. Finally, the Au or Ag counter electrode material is evaporated under vacuum.

The structure of planar heterojunction PSCs is shown in Figure 2(b), which contains FTO substrate/compact TiO_2 layer/perovskite light-absorption layer/HTL/counter electrode. Compared with meso-structured PSCs, there is no mesoporous TiO_2 scaffold in the planar heterojunction PSCs. Thus, the perovskite light-absorption material is directly spin-coated or deposited by vapor deposition and vapor-assisted solution processes on surface of the compact TiO_2 layer [9, 12]. The HTM and counter electrode are prepared by a method similar to the meso-structured PSCs.

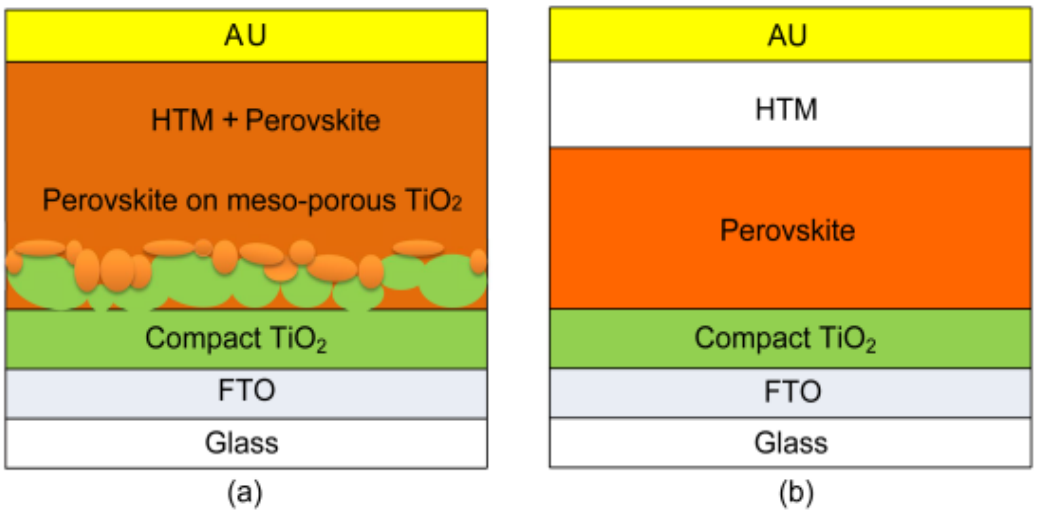

Figure 2. (a) The structural diagram of meso-structured PSCs and (b) planar heterojunction PSCs. (Reproduced with permission from ref. [32]).

2.2. Work principles of PSCs

The schematic of PSCs and energy diagram of titania, perovskite and HTM are shown in Figure 3 [38]. PSCs work on the basis that the perovskite absorbs certain wavelength range of sunlight which separates the electron-hole pairs [39]. The electrons are collected via electron transporting materials such as TiO_2 and then transferred to FTO while the holes transferred to the metal electrode via the HTM, through which the photocurrent is produced.

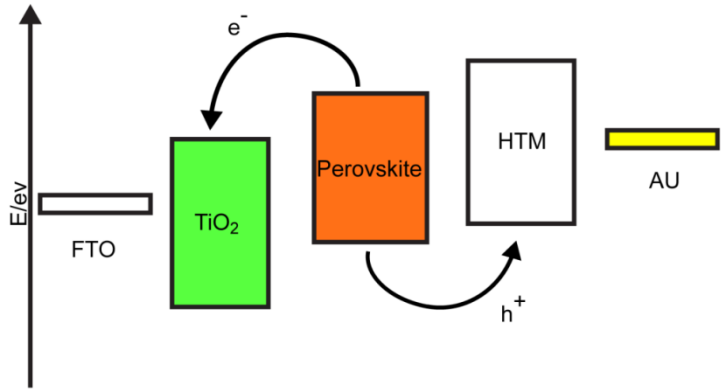

Figure 3. Schematic of PSCs and energy diagram of titania, perovskite and HTM. (Reproduced with permission from ref. [38]).

3. CRYSTAL STRUCTURE OF LIGHT-ABSOPTION MATERIAL OF PSCS

Generally, the formula of light-absorption material of PSCs is ABX_3, where $A=CH_3NH_2^+$, $HN=CHNH_3^+$ or Cs^+; $B=Pb^{2+}$ or Sn^{2+}; and $X=Cl^-$, Br^- or I^-. As shown in Figure 4 [40], the ideal crystal structure of perovskite is a cubic structure. The interstitial site of the perovskite cubic unit cell is occupied by the metal divalent cation B, while the lattice corners and lattice faces is occupied by cation A and the anion X, respectively. A metal divalent cation B and 6 anions X form BX_6 octahedra in which a cation B locates at its center. However, the actual structure of perovskite is not the ideal cubic crystal structure which is more stable than other crystal forms. Thus, the conception of tolerance factor was proposed by Goldschmidt in 1926, and it can be described by equation (1) [41]:

$$t=\frac{r_A+r_X}{\sqrt{2}(r_B+r_X)} \quad (1)$$

where t is the tolerance factor, r_A is the radius of cation A, r_B is the radius of cation B, and r_X is the radius of anion X.

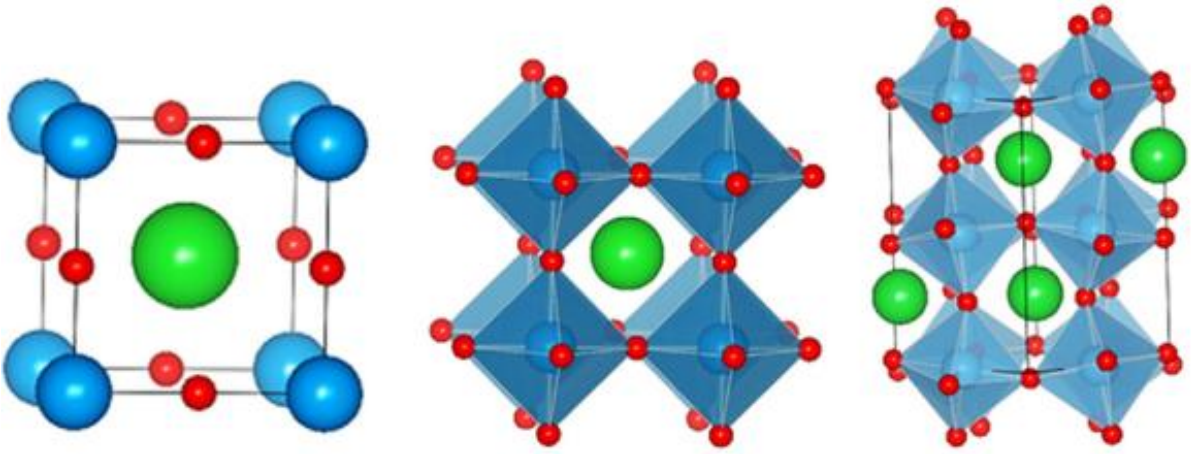

Figure 4. The ideal structure of perovskite: blue spheres stand for cation A, green spheres stand for cation B and red spheres stand for anion X. (Reproduced with permission from ref. [40]).

4. RESEARCH PROGRESS ON LESS LEAD PSCS

As mentioned above, the organic lead halide perovskite as the light-absorption material that is widely used in PSCs is mostly unfriendly to environment. Consequently, researchers attempted to fabricate the tin substitution for lead hybrid PSCs in order to avoid the lead component. Ogomi and his co-workers fabricated a less lead PSCs using $CH_3NH_3Sn_xPb_{(1-x)}I_3$ (x=0, 0.1, 0.3, 0.5, 0.7, 0.9 and 1) as the light-absorption material. The morphology of tin substitution for lead hybrid perovskite with different x ratios are shown in Figure 5 [42]. It can be seen that with the increase of x from 0 to 0.5, the rod-like organic lead halide perovskite turn to the flower-like tin substitution for lead hybrid perovskite. With further increase of the content of tin, the flower-like perovskite disappeared. Ogomi chose P3TH as HTM due to that the valence band of $CH_3NH_3Sn_xPb_{(1-x)}I_3$ is narrower than the most common HTM Spiro-OMeTAD. The device structure of the tin substitution for lead hybrid perovskite is FTO/compact TiO_2 layer/mesoporous TiO_2 layer/$CH_3NH_3Sn_xPb_{(1-x)}I_3$ light-absorption layer/P3TH/Au. The flower-like $CH_3NH_3Sn_{0.5}Pb_{0.5}I_3$ PSCs attained the optimal performance with a PCE of 2.37%, an open-circuit voltage (V_{oc}) of 0.32V, a short-current density (J_{sc}) of 19.88 $mA \cdot cm^{-2}$, and a fill factor (FF) of 0.37, respectively and the PCE reached 4.18% after optimization. Notably, the edge value of the incident photon to current efficiency (IPCE) reached 1060 nm in the near-infrared region (NIR) and 260nm red-shifting compared with the $CH_3NH_3PbI_3$. It is thought the flower-like morphology is beneficial for the high performance of PSCs perovskite. Similarly, we prepared flower-like nickel sulfides through an in-situ growth method and used them as counter electrodes to assemble dye-sensitized dye solar cells and obtained a PCE of 7.1%, which is better than nickel sulfides with other morphologies [43].

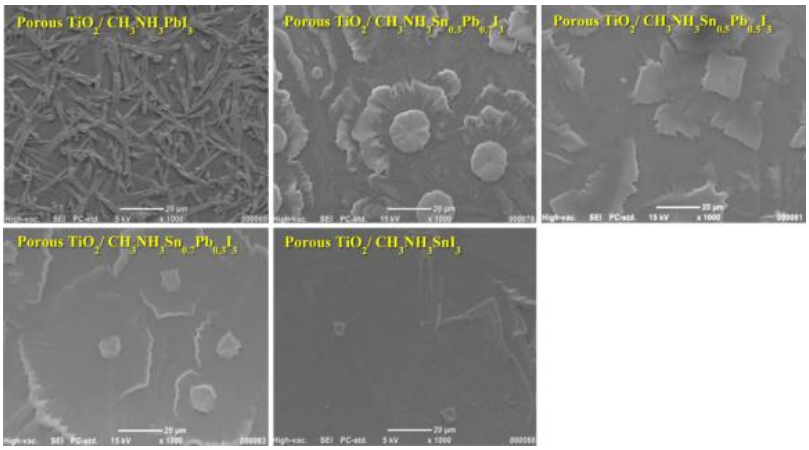

Figure 5. SEM micromorphologies of $CH_3NH_3Sn_xPb_{(1-x)}I_3$ on porous TiO_2 scaffold. (Reproduced with permission from ref. [42]).

Ogomi and his co-workers found that the addition of PbI_2 decreases the concentration of Sn^{4+} and carriers and reduces the probability of recombination of charges, which can be understood that the addition of Pb^{2+} restricted the oxidation of Sn^{2+} and consequently enhancing the stability of tin substitution for lead hybrid perovskite [42]. The highest V_{oc} of this type of PSC is only 0.32V which is

far lower than expectation. It was explained that charge recombination occurs at the boundary surfaces between ETL and perovskite layer and also between ETL and HTL [44-46]. Therefore, the surface defect of the TiO_2 layer need to be activated so as to improve the performance of tin substitution for lead hybrid PSCs.

Though the PCE of tin substitution for lead hybrid PSCs fabricated by Ogomi still needs to be improved, high light-absorption ability of this type of material is an attractive factor to be applied into the fabrication of solar cells. Its ability of working in the NIR region makes it possible to fabricate PSCs in series, which can not be fulfilled using $CH_3NH_3PbI_3$.

In order to attain a high efficiency, Spiro-OMeTAD need to be used as HTM since it plays an essential role in achieving a good performance in lead-based PSCs. Hao et al. fabricated meso-structured $CH_3NH_3Sn_xPb_{(1-x)}I_3$ tin substitution for lead hybrid PSCs by a solution method, adding lithium bis(trifluoromethylsulfonyl)imide (Li-TFSI) and pyridinium as additive to Spiro-OMeTAD as HTM. The current−voltage (*J*−*V*) curve is shown in Figure 6 [47]. The *J*-*V* curve suggested that the performance of $CH_3NH_3Sn_{0.5}Pb_{0.5}I_3$ PSCs is better than other cells, with the highest J_{sc} value of 20.64 $mA \cdot cm^{-2}$ and the second highest PCE value of 7.27% while the PCE of $CH_3NH_3Sn_{0.25}Pb_{0.75}I_3$ attained the maximum value of 7.37%. Nevertheless, the smaller FF value of tin substitution for lead hybrid PSCs than other highly efficient PSCs gives rise to a lower efficiency [48, 49]. This phenomenon is due to that the oxidation of Sn^{2+} leads to P type doping in the process of fabrication. Therefore, the FF value can be improved through efficient interface engineering which can restrict the recombination of charge and improve the cell efficiency.

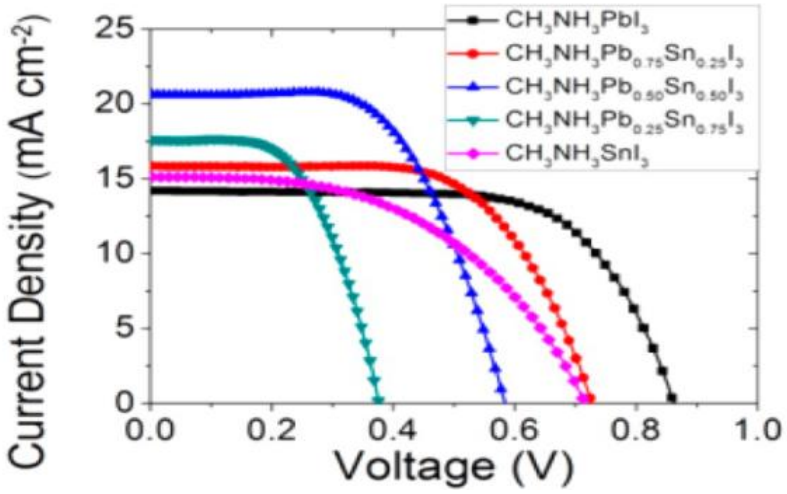

Figure 6. Photocurrent *J*-*V* characteristics of $CH_3NH_3Sn_xPb_{(1-x)}I_3$. (Reproduced with permission from ref. [47]).

Research on strontium substitution for lead hybrid PSCs have been reported by Bai et al. [50]. The stability of $CH_3NH_3Sr_xPb_{(1-x)}I_3$ was poor after a portion of lead was substituted by strontium due to change of band gap, which results in the mismatch of band gap between perovskite light-absorption material and HTM. Though the performance of strontium substitution for lead hybrid PSCs is not as

good as the strontium substitution for lead hybrid PSCs, new idea of synthesising other element substitution for lead hybrid perovskite material was evoked by Bai's research.

5. LEAD-FREE PSCS

As mentioned above, it is of great significance to fabricate lead-free PSCs though it is still a great challenge. Organic and inorganic hybrid tin-based perovskite such as $CH_3NH_3SnI_3$, $HC(NH_2)_2SnI_3$ and inorganic perovskite like $CsSnI_3$ have been reported as the light-absorption material in the lead-free PSCs, which are summarized in the following section.

5.1 Organic and Inorganic Hybrid Lead-Free PSCs

For organic and inorganic hybrid lead-free PSCs, $CH_3NH_3SnI_3$ is commonly used as the lead-free light-absorption material. Noel et al. demonstrated the first example of lead-free PSCs by utilizing $CH_3NH_3SnI_3$ as active material and attained a PCE of 6%, which is consisted of FTO/TiO_2 compact layer/TiO_2 mesoporous layer/$CH_3NH_3SnI_3$ light-absorption layer/Spiro-OMeTAD as HTM/Au [51]. Tert-butylpyridine (tBP) and hydrogen bis(trifluoromethanesulfonyl)imide (H-TFSI) as the additive were added to Spiro-OMeTAD [52, 53]. The function of tBP is to restrict the recombination of the charge. In addition, H-TFSI instead of the general additive Li-TFSI was used to improve the concentration of the charge in the HTL through the controlled experiments. The addition of HTM additives enhances the efficiency and stability of the PSCs [54]. Through controlling the process of crystalization, $CH_3NH_3SnI_3$ and $CH_3NH_3PbI_{(3-x)}Cl_x$ were attained [51]. The respective thin film and SEM images of the cross section are shown in Figure 7 [51]. It can be seen $CH_3NH_3PbI_{(3-x)}Cl_x$ film is smoother than $CH_3NH_3SnI_3$ film, and the compact degree of $CH_3NH_3SnI_3$ film that prepared on top of the 400-nm-thick mesoporous TiO_2 layer is better than that prepared on the 80-nm-thick mesoporous TiO_2 layer.

During preparation of the light-absorption material, $CH_3NH_3SnI_3$ would decay rapidly if the tin-based lead-free perovskite is exposed to ambient air condition. It means the tin-based perovskite material is extremely easily degraded under ambient air condition so the materials preparation and device assembly has to be carried out in an inert atmosphere in the glove box. Furthermore, the whole device needs to be encapsulated by hot-melt polymer film, a glass cover slide and the edge sealed with epoxy resin. In order to attain the authentic performance of tin-based PSCs, the encapsulation device was tested immediately after removing from the inertial condition. Therefore, the sensitivity to moisture and oxygen of tin-based perovskite are the main reasons that restrict their commercial application.

The first lead-free PSCs fabricated by Noel exhibited a PCE value of 6.4%. As a light-absorber with the band gap of 1.26eV, the V_{oc} value of 0.88V is comparable with the good results for highly efficient organic lead halide PSCs and the value for the voltage loss (the difference between the value of band gap and V_{oc}) is only 0.35V [55], which is also comparable with the voltage losses of c-Si. It means that the theoretical maximum PCE value of solar cells using $CH_3NH_3SnI_3$ as the light-

absorption material can rival with the c-Si and GaAs solar cells [56-58]. Nevertheless, Noel also found that the photoluminescence lifetime of the tin-based perovskite is far lower than the organic lead halide perovskite material [59-61], which is due to the easy oxidation of Sn^{2+} to Sn^{4+} that causes the P type self-doping which exacerbates the recombination of the charge. In addition, the value of J_{sc} and FF decrease with the aggravation degree of P type self-doping, so the $CH_3NH_3SnI_3$ as the light-absorption material has a promising prospects of exceeding the organic lead halide PSCs.

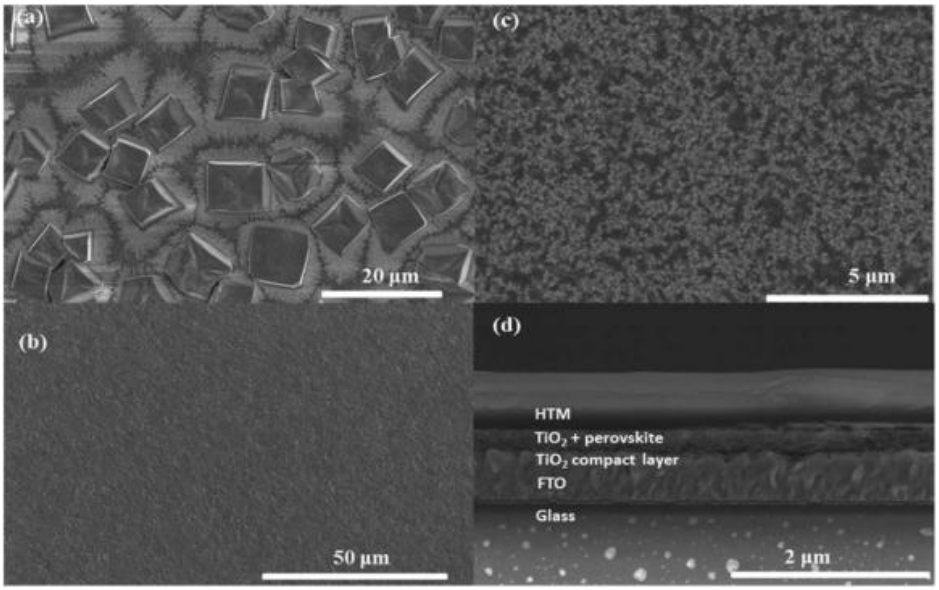

Figure 7. SEM images of (a) $CH_3NH_3SnI_3$ thin film on 80-nm-thick mesoporous TiO_2, (b) $CH_3NH_3PbI_{(3-x)}Cl_x$ thin film on 400-nm-thick mesoporous TiO_2, (c) $CH_3NH_3SnI_3$ thin film on 400-nm-thick mesoporous TiO_2 and (d) Cross-section of the cells. (Reproduced with permission from ref. [51]).

Enlightened by the morphology study of organic lead perovskite [12, 62, 63], Hao et al. applied solvent engeering to the one-step solution method to prepare the pinhole-free thin film of $CH_3NH_3SnI_3$ [64]. In the process of spin-coating step, uniform, non-pinhole and well-covered $CH_3NH_3SnI_3$ thin film was prepared by utilizing dimethyl sulfoxide(DMSO) and 20% SnF_2 as solvent through controlling solvent evaporation and the convective self-assembly process. The lead-free perovskite heterojunction depleted solar cells were fabricated and achieved a J_{sc} value of $21mA \cdot cm^{-2}$. Despite that the carriage concentration of $CH_3NH_3SnI_3$ PSCs is one order of magnitude higher than the organic lead PSCs, the recombination lifetime is comparable, indicating that the good-quality thin film of $CH_3NH_3SnI_3$ plays a positive role in the further improvement of PCE value. Hao et al. also reported a $CH_3NH_3SnI_{(1-x)}Br_x$ lead-free light-absorption material through a solution method, and they found that the value of V_{oc} and FF increase with the increasing ratio of Br while the value of J_{sc} shows the opposite trend [65]. $CH_3NH_3SnIBr_2$ PSCs displayed a promising PCE of 5.73% and the research on tunable engineering of halide element "X" broaden the research field of tin-based lead-free perovskite.

Considering the unstability of $CH_3NH_3SnI_3$, it is vital to develop a more stable lead-free perovskite. Koh et al. found that the organic cation $HC(NH2)_2^+$ can form stable hydrogen bonds with

inorganic section [66, 67], which could stabilize the phase of $HC(NH_2)_2BX_3$ under 150℃ [68, 69]. It suggests that $HC(NH_2)_2BX_3$ is more stable than $CH_3NH_3BX_3$ [70], and thus they fabricated $HC(NH_2)_2BX_3$ meso-structured perovskite solar cells. It is necessary to add SnF_2 into $HC(NH_2)_2SnI_3$ to obtain a smooth and non-pinhole $HC(NH_2)_2SnI_3$ thin film. From the $HC(NH_2)_2SnI_3$ surface SEM images with different concentrations of additive that are shown in Figure 8(a)-(c) [66], the coverage of $HC(NH_2)_2SnI_3$ with 20% SnF_2 on the top of mesoporous layer is the best. The well-covered $HC(NH_2)_2SnI_3$ thin film lowers the probability of charge recombination at the interface through solvent engineering [71]. Consequently, the $HC(NH_2)_2SnI_3$ PSCs with 20% SnF_2 additive performed the best. In the meantime, the thickness of TiO_2 mesoporous layer impact on the performance of the cell is studied. It is demonstrated that a proper thickness of TiO_2 mesoporous scaffold enhances the ability of light-absorption and also reduces the charge recombination; meanwhile, the 500-nm-thick TiO_2 mesoporous layer exhibited an enhanced performance. The device cross-sectional SEM image is shown in Figure 8(d) [66]. However, the optimizing PCE value is merely 2.1%, and thus $HC(NH_2)_2SnI_3$ is not the optimal light-absorption material for PSCs.

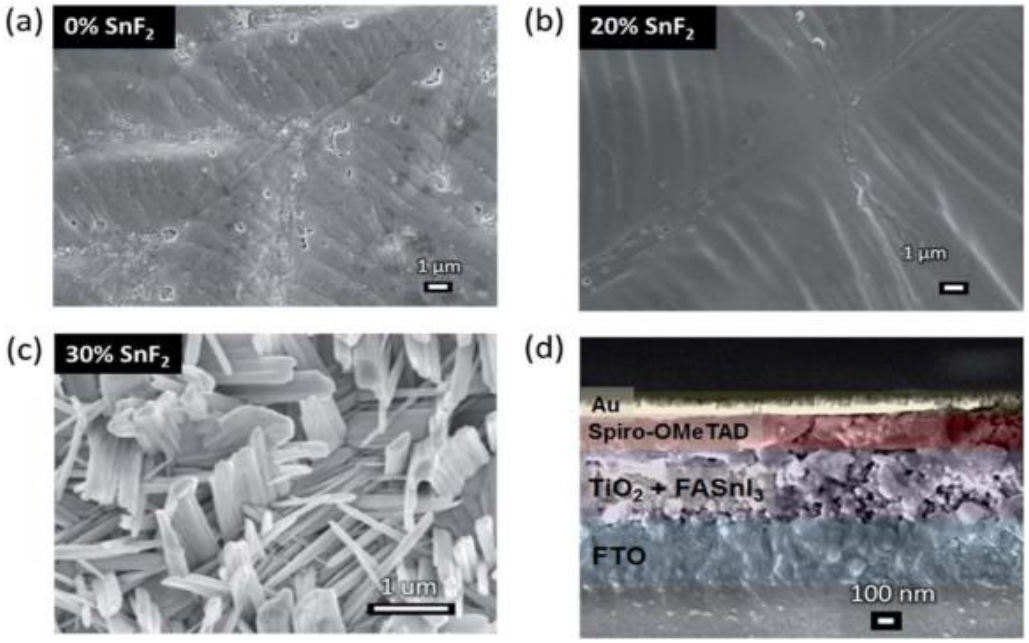

Figure 8. (a-c) SEM images of $FASnI_3$, $FASnI_3$: 20% SnF_2 and $FASnI_3$: 30% SnF_2 perovskite films deposited on the mesoporous TiO_2 layer and (d) SEM image of the cell cross-section. (Reproduced with permission from ref. [66]).

5.2 Inorganic metal halide Lead-Free PSCs

Organic and inorganic hybrid lead halide perovskite is currently the dominating light-absorption material in PSCs. Both organic-inorganic lead halide perovskite and inorganic tin halide perovskite $CsSnI_3$ possess suitable band gap, high light-absorption coefficient [72], and low exciton binding energy [73, 74]. Therefore, $CsSnI_3$ is the suitable light-absorption material. However, the conductivity of $CsSnI_3$ hinder its application in PSCs. Kumar et al. added certain concentration of SnF_2

to restrict its conductivity, making it possible to fabricate PSCs [75]. The meso-structured PSCs was fabricated through a solution method and 4,4′,4″-tris(N,N-phenyl-3-methylamino) triphenylamine (m-MTDATA) as HTM, which exhibited a high J_{sc} value of 22.7mA·cm^{-2} but both the PCE and V_{oc} are low. To increase the V_{oc}, Kumar substituted iodide ions with bromide ion in another report [76], both increasing the V_{oc} value and broaden the absorption scope. The perovskite materials reviewed above are unstable in the ambient air condition, so Saparov et al. assembled air-stable lead-free PSCs through two-step deposition to prepare $Cs_3Sb_2I_9$ light-absorption thin film [77]. $Cs_3Sb_2I_9$ perovskite shows an excellent air-stability that it stays pure when tested over 60 days after device completed while apparent decay can be observed within 5 days for general organic lead perovskite. It was attributed to the structural stability of inorganic perovskite and uneasy oxidation for Sb^{3+} compared with Sn^{2+}. However, the low J_{sc} value leads to poor performance of this device. The performances of different kinds of less-lead and lead-free PSCs are summarized in Table 1.

Table 1. A comparison of the performance of PSCs fabricated by different less-lead and lead-free absorption materials and HTM

Reference	Absorption material	HTM	J_{sc}/mA·cm^{-2}	V_{oc}/V	FF	PCE/%
[42]	$MASn_{0.5}Pb_{0.5}I_3$	P3TH	20.04	0.42	0.50	4.18
[47]	$MASn_{0.5}Pb_{0.5}I_3$	Spiro-OMeTAD+Li-TFSI	20.64	0.58	0.60	7.27
[50]	$MASr_{0.3}Pb_{0.7}I_3$	Spiro-OMeTAD+tBP	2.8	0.94	0.73	1.93
[51]	$MASnI_3$	Spiro-OMeTAD+(tBP,H-TFSI)	16.8	0.88	0.42	6.40
[65]	$MASnIBr_2$	Spiro-OMeTAD+Li-TFSI	12.3	0.82	0.57	5.73
[72]	$FASnI_3$+20%SnF_2	Spiro-OMeTAD	12.4	0.26	0.44	2.10
[75]	$CsSnI_3$+20%SnF_2	m-MTDATA	22.7	0.24	0.37	2.02

6. SUMMARY

In most of the published works on less-lead and lead-free PSCs so far, one-step solution method has been commonly used in fabricating meso-structured PSCs. Considering the light-absorption ability of material and device performance, tin is a promising element to substitute lead. However, the performance of less-lead and lead-free PSCs is still inferior to organic lead halide solar cells due to shortage of tin-based perovskite and research situation. Better stability and performance can be achieved through three aspects including the use of a suitable material, to prevent the oxidation of Sn^{2+} and to reduce the charge recombination. If breakthrough happens on the research on fabrication method, optimized device structure and applicable light-absorption materials of less-lead and lead-free PSCs, an environment-friendly, high efficient and renewable PSC is likely to be put into application.

ACKNOWLEDGEMENTS
This work was financially supported by the National Natural Science Foundation of China (No. 51374146 and 51602202), and the Shenzhen Dedicated Funding of Strategic Emerging Industry Development Program (No. 2014A030310323, JCYJ20160422112012739 and JCYJ20150324141711596)

References

1. G. Kilibarda, S. Schlabach, D.V. Szabó,T. Hanemann, *Int. J. Electrochem. Sci*., 10 (2015) 9988.
2. M. La, Y. Feng, C. Chen, C. Yang,S. Li, *Int. J. Electrochem. Sci.*, 10 (2015) 1563.
3. A.C. Mkhohlakali, P.A. Ajibade, *Int. J. Electrochem. Sci.*, 10 (2015) 9907.
4. A. Sedghi, H.N. Miankushki, *Int. J. Electrochem. Sci.*, 10 (2015) 3354.
5. C. Zhang, P. Zhang, S. Yun, Y. Li, T. He, *J. Inorg. Mater.*, 31 (2016) 113.
6. G. Hodes, *Science*, 342 (2013) 317.
7. A. Kojima, K. Teshima, Y. Shirai, T. Miyasaka, *J. Am. Chem. Soc.*, 131 (2009) 6050.
8. H.S. Kim, C.R. Lee, J.H. Im, K.B. Lee, T. Moehl, A. Marchioro, S.J. Moon, R. Humphry-Baker, J.H. Yum, J.E. Moser, M. Grätzel, N.G. Park, *Sci. Rep*., 2 (2012) 591.
9. M. Liu, M.B. Johnston, H.J. Snaith, *Nature*, 501 (2013) 395.
10. J. Burschka, N. Pellet, S.J. Moon, R. Humphry-Baker, P. Gao, M.K. Nazeeruddin, M. Grätzel, *Nature*, 499 (2013) 316.
11. J. Chang, H. Zhu, B. Li, F.H. Isikgor, Y. Hao, Q. Xu, J. Ouyang, *J. Mater. Chem. A*, 4 (2016) 887.
12. H. Zhou, Q. Chen, G. Li, S. Luo, T.B. Song, H.S. Duan, Z. Hong, J. You, Y. Liu, Y. Yang, *Science*, 345 (2014) 542.
13. J.W. Lee, D.H. Kim, H.S. Kim, S.W. Seo, S.M. Cho, N.G. Park, *Adv. Energy Mater*., 5 (2015) 1501310.
14. W.S. Yang, J.H. Noh, N.J. Jeon, Y.C. Kim, S. Ryu, J. Seo, S.I. Seok, *Science*, 348 (2015) 1234.
15. J. You, Z. Hong, Y.M. Yang, Q. Chen, M. Cai, T.B. Song, C.C. Chen, S. Lu, Y. Liu, H. Zhou, Y. Yang, *ACS Nano*, 8 (2014) 1674.
16. J.H. Heo, H.J. Han, D. Kim, T.K. Ahn, S.H. Im, *Energy Environ. Sci*., 8 (2015) 1602.
17. H. Zhang, J. Mao, H. He, D. Zhang, H.L. Zhu, F. Xie, K.S. Wong, M. Grätzel, W.C.H. Choy, *Adv. Energy Mater.*, 5 (2015) 1501354.
18. K. Mahmood, B.S. Swain, A. Amassian, *Nanoscale*, 7 (2015) 12812.
19. J.H. Im, I.H. Jang, N. Pellet, M. Grätzel, N.G. Park, *Nat. Nanotechnol*., 9 (2014) 927.
20. P. Docampo, J.M. Ball, M. Darwich, G.E. Eperon, H.J. Snaith, *Nat. Commun*., 4 (2013) 2761.
21. W. Chen, Y. Wu, J. Liu, C. Qin, X. Yang, I. Ashraful, Y.B. Cheng, L. Han, *Energy Environ. Sci*., 8 (2015) 629.
22. M. Grätzel, R.A. Janssen, D.B. Mitzi, E.H. Sargent, *Nature*, 488 (2012) 304.
23. X. Zhao, N.G. Park, *Photonics*, 2 (2015) 1139.
24. M. Saliba, T. Matsui, J.Y. Seo, K. Domanski, J.P. Correa-Baena, M.K. Nazeeruddin, S.M. Zakeeruddin, W. Tress, A. Abate, A. Hagfeldt, M. Grätzel, *Energy Environ. Sci*., 9 (2016) 1989.
25. I.R. Benmessaoud, A.L. Mahul-Mellier, E. Horváth, B. Maco, M. Spina, H.A. Lashuel, L. Forró, *Toxicol. Res*., 5 (2016) 407.
26. Y. Yang, J. Gao, J. Cui, X. Guo, *J. Inorg. Mater*., 30 (2015) 1131.
27. L. Guan, M. Li, X. Li, Z. Wei, F. Teng, *Chin. Sci. Bull.*, 60 (2015) 581.
28. C. Gu, B. Zhang, Y. Feng, *Prog. Chem.*, 28 (2016) 219.
29. X. Lu, Y. Zhao, J. Liu, C. Li, X. You, Chin. *J. Inorg. Chem*., 31 (2015) 1678.
30. C.C. Chueh, C.Z. Li, A.K.Y. Jen, *Energy Environ. Sci.*, 8 (2015) 1160.
31. P.P. Boix, K. Nonomura, N. Mathews, S.G. Mhaisalkar, *Mater. Today*, 17 (2014) 16.
32. M. Grätzel, *Nat. Mater.*, 13 (2014) 838.

33. S.A. Bretschneider, J. Weickert, J.A. Dorman, L. Schmidt-Mende, *APL Mater*., 2 (2014) 040701.
34. M. Ye, X. Hong, F. Zhang, X. Liu, *J. Mater. Chem. A*, 4 (2016) 6755.
35. M.A. Green, A. Ho-Baillie, H.J. Snaith, *Nat. Photon*., 8 (2014) 506.
36. S.D. Stranks, H.J. Snaith, *Nat. Nanotechnol.*, 10 (2015) 391.
37. G.E. Eperon, V.M. Burlakov, P. Docampo, A. Goriely, H.J. Snaith, *Adv. Funct. Mater.*, 24 (2014) 151.
38. J.A. Christians, R.C. Fung, P.V. Kamat, *J. Am. Chem. Soc.*, 136 (2014) 758.
39. S. Luo, W.A. Daoud, *J. Mater. Chem. A*, 3 (2015) 8992.
40. Q. Chen, N.D. Marco, Y.M. Yang, T.B. Song, C.C. Chen, H. Zhao, Z. Hong, H. Zhou, Y. Yang, *Nano Today*, 10 (2015) 355.
41. V.M. Goldschmidt, *Naturwissenschaften*, 14 (1926) 477.
42. Y. Ogomi, A. Morita, S. Tsukamoto, T. Saitho, N. Fujikawa, Q. Shen, T. Toyoda, K. Yoshino, S.S. Pandey, T. Ma, S. Hayase, *J. Phys. Chem. Lett*., 5 (2014) 1004.
43. C. Zhang, Y. Li, L. Deng, P. Zhang, X. Ren, S. Yun, *J. Solid State Electrochem.*, 20 (2016) 2373.
44. Y. Ogomi, S. Sakaguchi, T. Kado, M. Kono, Y. Yamaguchi, S. Hayase, *J. Electrochem. Soc*., 153 (2006) A2294.
45. Y. Ogomi, K. Kukihara, S. Qing, T. Toyoda, K. Yoshino, S. Pandey, H. Momose, S. Hayase, *Chemphyschem. Eur. J. Chem. Phys. Appl. Phys. Phys. Chem*., 15 (2014) 1062.
46. K. Kukihara, Y. Ogomi, Q. Shen, T. Saito, K. Yoshino, All Solid Dye-Sensitized Solar Cells with Perovskite Material, Taiwan, China, 2013.
47. F. Hao, C.C. Stoumpos, R.P.H. Chang, M.G. Kanatzidis, *J. Am. Chem. Soc*., 136 (2014) 8094.
48. A. Mancini, P. Quadrelli, C. Milanese, M. Patrini, G. Guizzetti, L. Malavasi, *Inorg. Chem.*, 54 (2015) 8893.
49. Y. Rong, L. Liu, A. Mei, X. Li, H. Han, *Adv. Energy Mater.*, 5 (2015) 1501066.
50. X. Bai, Y. Shi, K. Wang, Q. Dong, Y. Xing, H. Zhang, L. Wang, T. Ma, *Acta Phys. Chim. Sin*., 31 (2015) 285.
51. N.K. Noel, S.D. Stranks, A. Abate, C. Wehrenfennig, S. Guarnera, A.A. Haghighirad, A. Sadhanala, G.E. Eperon, S.K. Pathak, M.B. Johnston, A. Petrozza, L.M. Herz, H.J. Snaith, *Energy Environ. Sci.*, 7 (2014) 3061.
52. Y.S. Kwon, J. Lim, H.J. Yun, Y.H. Kim, T. Park, *Energy Environ. Sci.*, 7 (2014) 1454.
53. T. Leijtens, J. Lim, J. Teuscher, T. Park ,H.J. Snaith, *Adv. Mater.*, 25 (2013) 3227.
54. J. Krüger, R. Plass, L. Cevey, M. Piccirelli, M. Grätzel, U. Bach, *Appl. Phys. Lett.*, 79 (2001) 2085.
55. H.J. Snaith, *Adv. Funct. Mater*., 20 (2010) 13.
56. W. Shockley, H.J. Queisser, *J. Appl. Phys*., 32 (1961) 510.
57. M.A. Green, K. Emery, Y. Hishikawa, W. Warta, E.D. Dunlop, *Prog. Photovoltaics: Res. Appl*., 23 (2015) 1.
58. P.K. Nayak, J. Bisquert, D. Cahen, *Adv. Mater*., 23 (2011) 2870.
59. C.R. Kagan, D.B. Mitzi, C.D. Dimitrakopoulos, *Science*, 286 (1999) 945.
60. S.D. Stranks, G.E. Eperon, G. Grancini, C. Menelaou, M.J.P. Alcocer, T. Leijtens, L.M. Herz, A. Petrozza, H.J. Snaith, *Science*, 342 (2013) 341.
61. G. Xing, N. Mathews, S. Sun, S.S. Lim, Y.M. Lam, M. Grätzel, S. Mhaisalkar, T.C. Sum, *Science*, 342 (2013) 344.
62. Y. Wu, A. Islam, X. Yang, C. Qin, J. Liu, K. Zhang, W. Peng, L. Han, *Energy Environ. Sci.*, 7 (2014) 2934.
63. N.J. Jeon, J.H. Noh, Y.C. Kim, W.S. Yang, S. Ryu, S.I. Seok, *Nat. Mater.*, 13 (2014) 897.
64. F. Hao, C.C. Stoumpos, P. Guo, N. Zhou, T.J. Marks, R.P.H. Chang, M.G. Kanatzidis, *J. Am. Chem. Soc*., 137 (2015) 11445.
65. F. Hao, C.C. Stoumpos, D.H. Cao, R.P.H. Chang, M.G. Kanatzidis, *Nat. Photon*., 8 (2014) 489.
66. T.M. Koh, T. Krishnamoorthy, N. Yantara, C. Shi, W.L. Leong, P.P. Boix, A.C. Grimsdale, S.G. Mhaisalkar, N. Mathews, *J. Mater. Chem. A*, 3 (2015) 14996.

67. P.P. Boix, S. Agarwala, T.M. Koh, N. Mathews, S.G. Mhaisalkar, *J. Phys. Chem. Lett*., 6 (2015) 898.
68. G.E. Eperon, S.D. Stranks, C. Menelaou, M.B. Johnston, L.M. Herz, H.J. Snaith, *Energy Environ. Sci*., 7 (2014) 982.
69. S. Pang, H. Hu, J. Zhang, S. Lv, Y. Yu, F. Wei, T. Qin, H. Xu, Z. Liu, G. Cui, *Chem. Mater.*, 26 (2014) 1485.
70. J.W. Lee, D.J. Seol, A.N. Cho, N.G. Park, *Adv. Mater.*, 26 (2014) 4991.
71. Y.C. Shih, L.Y. Wang, H.C. Hsieh, K.F. Lin, *J. Mater. Chem. A*, 3 (2015) 9133.
72. K. Shum, Z. Chen, J. Qureshi, C. Yu, J.J. Wang, W. Pfenninger, N. Vockic, J. Midgley, J.T. Kenney, *Appl. Phys. Lett.*, 96 (2010) 221903.
73. Z. Chen, C. Yu, K. Shum, J.J. Wang, W. Pfenninger, N. Vockic, J. Midgley, J.T. Kenney, *J. Lumin.*, 132 (2012) 345.
74. S. Dharani, H.K. Mulmudi, N. Yantara, P.T.T. Trang, N.G. Park, M. Grätzel, S. Mhaisalkar, N. Mathews, P.P. Boix, *Nanoscale*, 6 (2014) 1675.
75. M.H. Kumar, S. Dharani, W.L. Leong, P.P. Boix, R.R. Prabhakar, T. Baikie, C. Shi, H. Ding, R. Ramesh, M. Asta, M. Grätzel, S.G. Mhaisalkar, N. Mathews, *Adv. Mater*., 26 (2014) 7122.
76. D. Sabba, H.K. Mulmudi, R.R. Prabhakar, T. Krishnamoorthy, T. Baikie, P.P. Boix, S. Mhaisalkar, N. Mathews, *J. Phys. Chem. C*, 119 (2015) 1763.
77. B. Saparov, F. Hong, J.P. Sun, H.S. Duan, W. Meng, S. Cameron, I.G. Hill, Y. Yan, D.B. Mitzi, *Chem. Mater.*, 27 (2015) 5622.